Contrib Mineral Petrol (2004) 146: 566–576
DOI 10.1007/s00410-003-0518-2

ORIGINAL PAPER

D. E. Jacob · A. Kronz · K. S. Viljoen

Cohenite, native iron and troilite inclusions in garnets from polycrystalline diamond aggregates

Received: 10 March 2003 / Accepted: 1 September 2003 / Published online: 5 November 2003

Abstract Syngenetic garnet of eclogitic/pyroxenitic composition included in a polycrystalline diamond aggregate from the Venetia kimberlite, Limpopo Belt, South Africa shows multiple inclusions of spherules consisting of 61 ± 5 vol% Fe_3C (cohenite), 30 ± 2 vol% Fe-Ni and 9 ± 3 vol% FeS (troilite). Troilite forms shells around the native iron-cohenite assemblage, implying that both compositions were immiscible melts and were trapped rapidly by the silicate. It is proposed that this polycrystalline diamond-silicate-metallic spherule assemblage formed in very local pressure and fO_2 conditions in cracks at the base of the subcratonic lithosphere from a C-H-O fluid that reacted with surrounding silicate at about 1,300–1,400 °C. In a mantle fluid consisting of $CH_4 > H_2O > H_2$ near $fO_2 = IW$, the H_2 activity increases rapidly when carbon from the fluid is consumed by diamond precipitation, driving the oxygen fugacity of the system to lower values along the diamond saturation curve. Water from the fluid induces melting of surrounding silicate material, and hydrogen reduces metals in the silicate melt, reflected by an unusually low Ni content of the garnet. The carbon isotopic composition of $\delta^{13}C = -13.69‰$ (PDB) and the lack of nitrogen as an impurity is consistent with formation of the diamond from non-biogenic methane, whereas $\delta^{18}O = 7.4‰$ (SMOW) of the garnet implies derivation of the silicate from subduction-related material. Hence, very localized and transient reducing conditions within the subcratonic lithosphere can be created by this process and do not necessarily call for involvement of fluids derived from subducted material of biogenic origin.

Editorial responsibility: J. Hoefs

D. E. Jacob (✉)
Institut für Geologische Wissenschaften, Universität Greifswald,
F.L. Jahnstr. 17a, 17487 Greifswald, Germany
E-mail: djacob@uni-greifswald.de

Present address: D. E. Jacob
Max-Planck Institut für Chemie,
Abt. Geochemie, Postfach 3060, 55020 Mainz, Germany

A. Kronz
Geowissenschaftliches Zentrum der Universität Göttingen,
Goldschmidt-Str. 1, 37077 Göttingen, Germany

K. S. Viljoen
Geoscience Center, DeBeers Consolidated Mines, PO Box 82232,
Southdale 2135, South Africa

Introduction

Iron-carbide (cohenite) and iron have been reported as inclusions in diamonds, either isolated (Sharp 1966; Sobolev et al. 1989; Stachel et al. 1998) or intergrown with graphite (Bulanova and Zayakina 1990). At pressures close to or at atmospheric pressure, natural cohenite-native iron parageneses are known from basaltic rocks from Disko Island, Greenland (Goodrich and Bird 1985; Ulff-Møller 1985) and from the Hessian Depression, Germany (Irmer 1920). In commercial steel production, controlled iron carbide (''cementite'') formation plays an important role in the properties of steel and cast iron materials. Cohenite and native iron included in silicates from within the diamond stability field, however, have not been described previously. Many framesites have been found to be magnetic (Gurney and Boyd 1982; McCandless et al. 1989), but for the majority of cases, the magnetic minerals have not been identified (Collinson 1998). Cohenite and metallic iron are both carrier phases of remanent magnetism and could account for the unidentified magnetic inclusions in framesites.

Polycrystalline aggregates of diamond (boart, Orlov 1977; or framesite, Gurney and Boyd 1982) may interstitially enclose syngenetic minerals of peridotitic or eclogitic affinity, similar to syngenetic inclusions in gem-sized diamonds, but boart and framesite are much rarer than gem-sized diamonds and do not occur in every diamond-bearing kimberlite. Earlier studies on polycrystalline diamond and their inclusions show evidence

for variable age (Jacob et al. 2000) and conditions of formation (Dobosi and Kurat 2002; Kirkley et al. 1995; Kurat and Dobosi 2000; McCandless et al. 1989). In contrast to gem-sized diamonds, which are as likely to form from fluids as from melts, the characteristically high porosity of boart is evidence that this variety of diamond predominantly formed from C-H-O fluids. Compared to the often complex growth history of diamonds (Bulanova 1995), polycrystalline aggregates crystallize rapidly, and may provide fresh "snapshots" of the variability or the evolving conditions during diamond forming processes in the subcratonic lithosphere (Jacob et al. 2000). However, the inclusion chemistry of polycrystalline diamond aggregates differs from that in gem-sized stones (e.g. Sobolev et al. 1975), and suggests that the further record special, maybe rarer or more localized conditions of diamond growth.

Evidence from inclusions in gem-sized stones shows that many diamonds form in a rather narrow range of fO_2 around the IW oxygen buffer, but diamond formation conditions also extend to more oxidising as well as to more reducing regions (Navon 1999). In contrast, the Earth's mantle lithosphere in general is thought to be relatively oxidized in large parts, with fO_2 approximating that of the fayalite-magnetite-quartz (FMQ) oxygen buffer (Eggler 1983; O'Neill and Wall 1987). However, some parts may be as reduced as the iron-wüstite (IW) oxygen buffer (Haggerty and Tompkins 1986). Indications for much more reducing conditions during diamond formation of 6 log units below IW come from rare occurrences of moissanite (SiC: Leung et al. 1990; Mathez et al. 1995; Moore and Gurney 1986). The oxygen fugacity of the cohenite – native iron paragenesis cannot be calculated exactly, but clearly represents a reducing assemblage below the IW oxygen buffer or close to it. Unusually reducing conditions during diamond formation are sometimes used to argue in favour of an involvement of subduction-derived fluids of biogenic origin (e.g. Nisbet et al. 1994). Here, it will be shown that those conditions can be *created* locally in the upper mantle by redox processes where a normal mantle fluid interacts with its silicate environment.

Sample description

The studied sample (V906) belongs to a suite of polycrystalline diamond aggregates from the Venetia kimberlite pipe situated in the Limpopo central belt in north eastern South Africa (Allsopp et al. 1995) and weighs 2.9 g (14.4 cts). The diamond is primarily octahedral or, in dense intergrowths, irregularly shaped and encloses about 30 vol% interstitial garnet as the only silicate mineral. Parts with larger octahedral crystals and higher porosities are correctly addressed as boart (Orlov 1977), whereas regions of dense irregular intergrowth are framesite. Cogenetic crystallization of garnet is demonstrated by occasional inclusions of octahedral diamond within the garnet. After breaking, it could be seen that the majority of garnet grains contained numerous inclusions of round or ovoid black spherules ranging in size between ca. 1 and 50 μm (Fig. 1a, b), whereas other grains were visibly inclusion-free. Unlike equally black sulphide inclusions, commonly found in association with diamond, partly liberated metallic spherules in garnet grains split open by crushing appear completely round and unaffected by the crushing (Fig. 2). Some metallic spherules have small cavities at the spherule-garnet interface that we interpret as shrinkage bubbles (Fig. 2a). In one case, a spherule nucleated around a small octahedral diamond. Occasionally, native iron or troilite (FeS) is observed along cracks in the garnet (Fig. 1b). Some spherules, mostly positioned on cracks within garnet or exposed on the garnet surface, consist of a more coarse-grained graphite-native iron intergrowth, indicative of decomposition of cohenite following the reaction $Fe_3C = 3Fe + C$. The majority of spherules, however, are very fresh. All fresh spherules have an outer shell consisting of troilite (FeS), sometimes (in small spherules) completely covering the metallic part of the spherules. Troilite is also present as small rounded inclusions within the spherules. In two of the twenty-six spherules studied in detail, a small grain

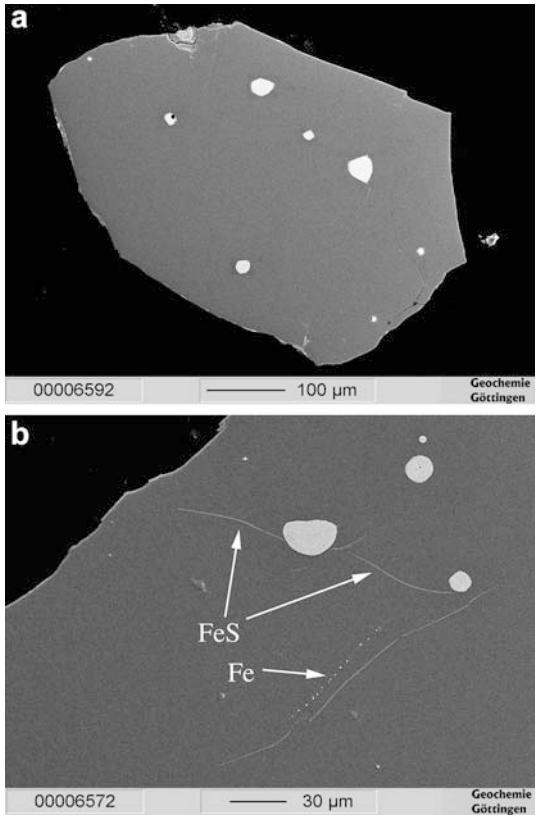

Fig. 1 Back-scattered electron image of polished garnet grains (*grey*) showing multiple metallic spherules (*light grey*). Native iron and troilite can be found disseminated along cracks in the silicate (**b**), sometimes leading to spherules in which the cohenite-native iron paragenesis is decomposed to a native iron and graphite assemblage. **a** shows a spherule of this assemblage at the upper rim

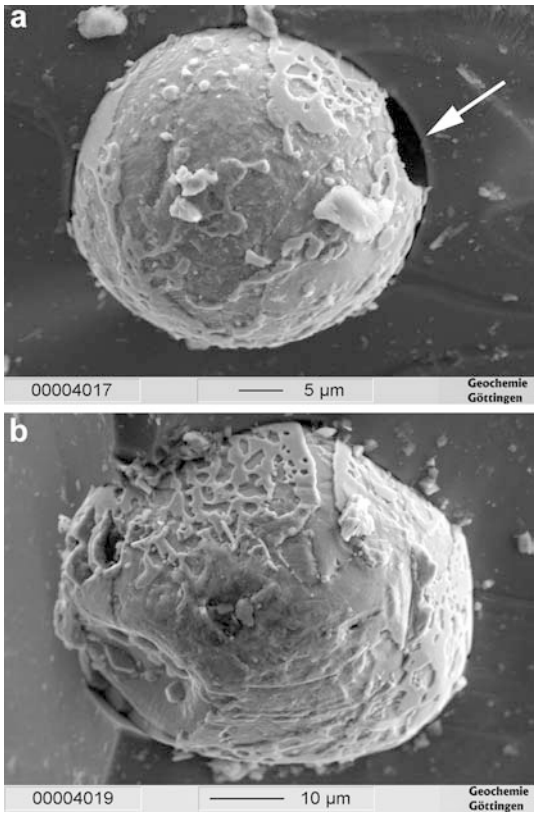

Fig. 2 Secondary-electron images of partly exposed spherules in garnet matrix. Note the shrinkage bubble at the spherule-silicate interface (*arrow*) and the net-like texture of the incomplete troilite shell around the metallic core

of chalcopyrite ($CuFeS_2$) was observed within the outer troilite shell. The inner part of the spherules consists of an intergrowth of cohenite (Fe_3C) and metallic Ni-bearing iron crystals of similar grain size (< 2 µm) intergrown with rounded troilite grains of up to 1 µm in size (Fig. 3a, b). Estimation of the modal abundances of the phases based on elemental phase mapping by electron microprobe carried out on eight individual spherules yielded 61 ± 5 vol% cohenite, 30 ± 2 vol% Fe-Ni and 9 ± 3 vol% troilite (2σ errors). Relatively large uncertainties arise partly from varying sectioning level of the spherules. This is especially so for troilite, since larger spherules often have an incomplete outer shell consisting of troilite, whereas smaller ones have a larger apparent troilite to metal ratio.

Sample preparation and analytical methods

The diamonds were wrapped in plastic to avoid direct contact with metal, and then carefully crushed, following which suitable grains of garnet with multiple black inclusions were handpicked under a binocular microscope. For electron microprobe analysis samples were mounted in EPOXY-resin (STRUERS GmbH, Germany), with samples and standards together in the same 1-in. mount. The hardened mount was ground with SiC (500, 1,000, 1,200 mesh), and then polished with a diamond-suspension with successive grain sizes of 3, 1 and 0.25 µm. After careful ultrasonic cleaning using tensides and water, the sample mount was dried under high vacuum using Ar-sputtering to avoid any surface contamination caused by hydrocarbons.

Chromium-metal (Alpha products, 38494, 99.995% purity) was chosen for coating due to its low absorption coefficient of 10,600 cm^2g^{-1} for C-Kα x-rays (Henke et al. 1982). Coat thickness was about 110 to 120 Å and was controlled using a quartz frequency sensor (Cressington MTM10). The measured thickness gives about 13.2% absorption (120 Å) of the initially produced C-Kα x-rays, as calculated by the Lambert-Beer equation.

Microprobe analyses of cohenite and garnet were performed using a JEOL JXA 8900 RL instrument in Göttingen, equipped with five WDS spectrometers and an EDS system. For high-precision measurement of carbon we use a V/C multilayer pseudocrystal (LDEC, 2d spacing = approx. 100 Å which gives count rates about 18 times higher compared to a conventional LDE1-multilayer (W/Si, 2d = 60 Å) due to its low absorption of C-Kα x-rays (as measured on diamond). For exciting x-rays of Fe, Co, Ni and Cu Kα an accelerating voltage of 15 kV is essential, despite the fact that this is not ideal for the excitation-range of carbon (phi-rho-Z distribution). A 20 nA beam current was chosen (measured on Faraday-cup) with highest possible focussing due to the small structures within the Fe_3C grains.

C and Fe were calibrated on highly stoichiometric cohenite from Disko, Greenland (Goodrich and Bird 1985). Pure Fe_3C from a technical cast-iron was measured as an unknown, giving stoichiometric results with a relative standard deviation (1σ) of 1.5% for C and 0.5% for Fe (relative error by counting statistics: 0.9% for C and 0.4% for Fe, 1 σ). Garnets were analysed using an accelerating voltage of 20 kV and a beam current of 20 nA (Faraday) with focussed beam. Standards, counting times, statistic errors (2-σ of the averaged counting statistic error) and detection limits for Fe, Fe_3C and garnet are given in Table 1. The sampling volume of the generated characteristic x-rays was calculated for both C-Kα and Fe-Kα using a Monte Carlo simulation (Newbury and Myklebust 1995). For an assumed density of 7.4 g/cm^3 and the accelerating voltage used the maximum depth (99% of sampled photons) amounts to 680 nm for C-Kα and 500 nm for Fe-Kα. Back-scattered and secondary electron images were performed using an accelerating voltage of 15 kV and a beam current of 0.05–0.1 nA. Nickel concentrations in garnet were measured in situ by Laser Ablation ICP-MS (Jacob et al. 2000, and references therein). Oxygen isotopes were measured by laser fluorination technique at Royal Holloway University of London (Mattey and Macpherson 1993), and carbon isotopes were measured using standard methods at IPGP, Université Paris.

Results

The chemical composition of cohenite (Table 2) is similar to that reported for terrestrial and meteoritic cohenites (Goodrich and Bird 1985; Lovering 1964). It has a carbon content of 6.53 wt% that varies within 8% (2σ) of that of stoichiometric cohenite (6.67 wt%). As cohenite is always stoichiometric (Petch 1944), this variation reflects the measurement quality, which is in turn largely influenced by intergrowth of the phases on a scale smaller than the average diameter of the excited volume of the penetrating electron beam. Nickel contents in cohenite vary between 1.13 and 2.21 wt%. Relatively high C and Ni contents (Table 2) identify the metallic Fe-Ni as γ-Fe, although variations in C, Ni and P contents (0.9–2.2%, 1.3–3.8%, and 0.08–0.61 wt%, respectively) imply the presence of irresolvable, but distinct high C, Ni (γ-Fe) and low C, Ni (α-Fe) phases (similar to the observations of Goodrich and Berkley 1986), as well

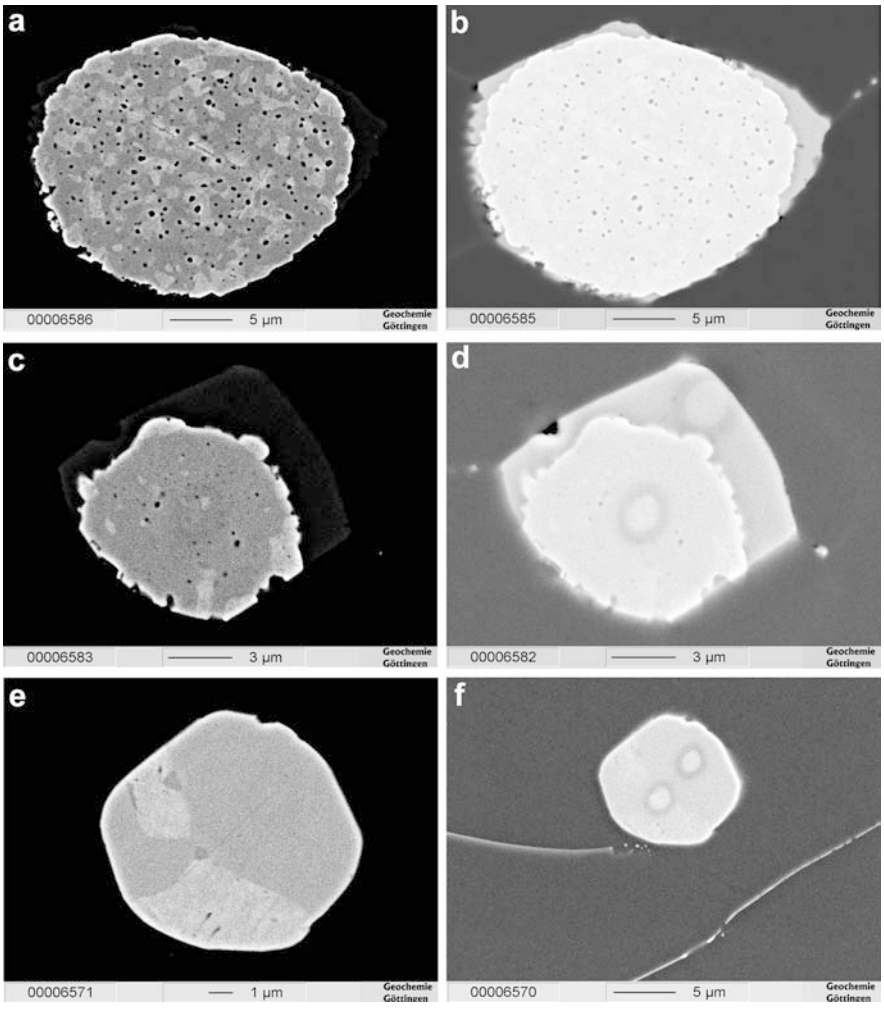

Fig. 3 Back-scattered electron images of polished spherules in garnet matrix. **a** to **d** are from the garnet grain in Fig. 1a; **e** and **f** are from the grain in Fig. 1b. In **b**, **d** and **f** the contrast is set so that the cohenite (*dark grey*) and native iron (*light grey*) crystals are visible and the troilite rim is not. The *black spots* in these figures are troilite grains within the metallic spherule cores, but light rims around them are artefacts caused by the strong difference in contrast. The *light spots with grey halo* in **c** and **e** are traces of the microprobe beam. The *light lines* in **e** are cracks filled with sulphide. Note that the smaller spherule in **c** has a wider apparent sulphide shell than the larger spherule **a**

Table 1 Standards, counting times, statistic errors (2σ of the averaged counting statistic error) and detection limits for Fe and Fe_3C (a) and garnet (b)

Element		Standard	Wt%	Peak (s)	Backgr.(s)	Det. Limit (ppm)	Error (ppm)
(a)							
1	Si	Si-metal	100.00	60	30	120	100
2	C	Fe_3C	6.69	30	15	810	1,230
3	S	ZnS, synthetic	32.90	30	15	110	190
4	Fe	Fe_3C	92.41	15	5	420	7,020
5	Co	Co-metal	100.00	60	30	370	290
6	P	Apatite	18.43	30	15	210	340
7	Ni	Ni-metal	100.00	30	15	490	900
8	Cu	Cu-metal	100.00	30	15	530	450
(b)							
1	SiO_2	Wollastonite	51.51	16	8	400	2,270
2	Na_2O	Albite	11.74	16	8	470	300
3	CaO	Wollastonite	47.74	16	8	170	830
4	TiO_2	TiO_2, synthetic	100.00	16	8	260	250
5	FeO	Hematite	89.72	16	8	230	1,040
6	Al_2O_3	Al_2O_3, synthetic	100.00	16	8	330	1,730
7	MgO	Garnet, USNM143968	18.51	16	8	320	1,570
8	K_2O	Orthoclase	14.67	16	8	300	200
9	Cr_2O_3	Cr_2O_3, synthetic	100.00	60	30	150	130
10	MnO	Rhodonite	42.44	30	15	180	200
11	NiO	NiO, synthetic	100.00	30	15	240	170

Table 2 Average EMP analyses of individual phases in metallic spherules and alloy bulk compositions calculated using an estimated mode of 61% cohenite, 30% Fe-Ni and 9% FeS. Analyses were carried out on mounted polished garnet grains containing spherules. n.d. = not detected

	Fe-Ni 1	Fe-Ni 2	Fe-Ni 3	Fe-Ni 4	Fe-Ni 5	Average Fe-Ni ($n=5$)	Coh1	Coh2	Coh3	Coh4	Coh5	Coh6	Coh7	Coh8	Coh9	Coh10	Coh11	Coh12	Coh13	Coh14	Average Cohenite ($n=14$)	Troi-1	Troi-2	Troi-3	Troi-4	Average Troilite ($n=4$)	Bulk metal (wt%)	Bulk metal (mol%)
Fe	94.10	95.69	96.33	95.69	92.44	94.85	90.46	90.29	90.39	90.21	91.05	89.63	89.24	90.34	89.85	91.13	91.32	90.92	89.39	91.52	90.41	61.26	61.14	61.73	61.73	61.47	89.14	75.14
Ni	2.42	2.68	1.26	2.59	3.80	2.55	1.56	1.77	1.63	1.60	1.31	1.74	1.68	2.21	1.89	1.22	1.4	1.13	2.16	1.25	1.61	0.080	0.043	0.027	0.044	0.05	1.75	1.41
Co	0.72	0.80	0.41	0.73	0.83	0.70	0.327	0.357	0.353	0.361	0.314	0.36	0.356	0.472	0.528	0.338	0.387	0.318	0.308	0.36	0.37	0.01	0.01	n.d.	n.d.	0.01	0.43	0.35
Cu	0.05	0.10	0.11	0.16	0.09	0.10	n.d.	0.055	0.075	n.d.	n.d.	0.054	0.032	0.056	0.050	0.049	0.062	0.080	0.067	n.d.	0.05	0.111	0.255	0.191	0.285	0.211	0.08	0.06
C	2.15	1.12	1.88	0.72	0.89	1.35	6.63	6.73	6.30	6.77	6.37	6.30	6.52	6.58	6.60	6.70	6.50	6.52	6.22	6.71	6.53	1.25	1.18	1.38	1.22	1.26	4.50	17.65
Si	0.02	0.02	0.03	0.03	0.04	0.03	0.041	0.024	0.032	0.034	0.032	0.030	0.026	0.036	n.d.	n.d.	n.d.	n.d.	n.d.	n.d.	0.03	0.089	0.097	0.388	0.240	0.204	0.04	0.07
P	0.10	0.08	0.61	0.10	0.33	0.24	0.489	0.588	0.531	0.257	0.145	0.364	0.294	0.443	0.243	0.220	0.310	0.218	0.982	0.286	0.384	0.029	n.d.	0.014	0.015	0.015	0.31	0.47
S	0.27	0.11	n.d.	0.04	0.13	0.11	0.083	0.188	0.198	0.181	0.070	0.212	0.111	0.202	0.185	0.225	0.539	0.339	0.204	0.212	0.211	35.13	35.17	34.54	34.99	34.96	3.31	4.56
Total	99.8	100.6	100.6	100.0	98.5	99.9	99.63	100.00	99.51	99.43	99.30	98.69	98.26	100.34	99.37	99.89	100.54	99.54	99.35	100.37	99.6	97.96	97.90	98.27	98.52	98.16	99.6	99.7

as of micro-inclusions of schreibersite (Fe_3P). The troilite has a relatively high average C content of 1.26 wt% (Table 2), which may be an artefact caused by secondary fluorescence during measurements.

Garnet is homogeneous (Table 3) with low Cr_2O_3 and low CaO contents and plots in the uppermost part of the websteritic field, close to the eclogite field (cf. Aulbach et al. 2002). However, a significant proportion of eclogitic garnets have CaO contents below 6 wt%, and, since no orthopyroxene (or other silicate phase) is present in the sample, this classification is somewhat ambiguous. The $\delta^{18}O$ value of $7.2 \pm 0.1‰$ (SMOW) may be more indicative of an eclogitic paragenesis rather than a websterite.

The Ni content of this garnet of 4.8 ppm is unusually low and lies about an order of magnitude below the average Ni content of eclogitic garnets from xenoliths (between 19.9 and 65 ppm; Jacob and Foley 1999, Jacob et al. 2003). It will be argued below that this unusually low Ni content is caused by preferential partitioning into the metallic spherules. No heterogeneities of major or trace elements, as described for other polycrystalline diamond aggregates (Jacob et al. 2000; Kurat and Dobosi 2000) could be detected and it should be noted that stoichiometric requirements indicate that Fe^{3+} amounts are negligible. The $\delta^{13}C$ value of $-13.7‰$ (PDB) of the diamond is in the range of those reported for diamonds from Venetia (-2.70 to $-18.0‰$; Deines et al. 2001; Jacob et al. 2000). Nitrogen concentration was below detection limits.

Discussion

Petrography and bulk composition of the metallic spherules bear similarities with those described from ureilites by Goodrich and Berkley (1986). Although the ureilitic spherules are generally larger (up to 150 μm), they too show characteristic outer shells of troilite whose apparent thickness is anticorrelated with spherule size. Goodrich and Berkley (1986) give a bulk metal estimate of 61 wt% Fe_3C, 31 wt% FeNi and 8 wt% FeS that is virtually identical to the estimate given in this study (Table 2). However, in contrast to the meteoritic metallic spherules, no large cohenite crystals are observed and bulk Ni contents are lower (1.75 wt% as opposed to 5–6 wt%), consistent with the more evolved composition of the eclogitic/pyroxenitic paragenesis. In comparison, white cast iron (WCI, Ulff-Møller 1985) from Disko Island, Greenland has a bulk composition of 44 wt% Fe_3C, 4 wt% FeS, 3 wt% wüstite and 48 wt% Fe with traces of schreibersite and pentlandite.

To adequately describe the metallic system, only Fe, C, S and Ni have to be taken into account, as all others (P, Co, Cu) are not abundant enough to affect the system. Only the Fe-C phase relations have been studied at high pressures (Strong and Tuft 1973; Wood 1993), whereas the effects of Ni and S are known only at

Table 3 Exemplary single analyses and average major element composition with 1σ standard deviation of eclogitic garnet V906 as determined by electron microprobe. $Mg\# = (Mg/[Mg + Fe^{2+}])*100$

	Grt1	Grt2	Grt3	Grt4	Grt5	Grt6	Grt7	Grt8	V906 gt ($n = 16$)	1σ
SiO_2	41.98	41.61	41.49	41.88	41.82	41.81	41.59	41.59	41.74	0.18
TiO_2	0.212	0.185	0.159	0.217	0.196	0.202	0.177	0.200	0.187	0.02
Al_2O_3	23.49	23.29	23.35	23.58	23.48	23.39	23.23	23.40	23.41	0.17
Cr_2O_3	0.16	0.138	0.145	0.142	0.145	0.202	0.202	0.16	0.168	0.02
FeO	9.41	9.36	9.41	9.45	9.30	9.38	9.38	9.42	9.36	0.06
MnO	0.357	0.363	0.348	0.361	0.351	0.357	0.339	0.335	0.352	0.01
MgO	17.77	18.01	18.07	17.98	18.06	18.09	18.25	17.88	17.92	0.21
CaO	6.02	6.04	6.04	6.08	6.00	5.82	5.83	5.98	5.96	0.08
Na_2O	n.d.	n.d	n.d.	n.d.	n.d.	n.d.	n.d.	n.d.	n.d.	
K_2O	n.d.	n.d.	n.d.	n.d.	n.d.	n.d.	n.d.	n.d.	n.d.	
Total	99.43	99.03	99.07	99.69	99.36	99.26	99.01	99.01	99.12	0.25
Si	3.014	3.002	2.993	3.001	3.004	3.007	3.000	3.001	3.007	
Ti	0.011	0.010	0.009	0.012	0.011	0.011	0.010	0.011	0.010	
Al	1.988	1.980	1.985	1.991	1.988	1.982	1.975	1.990	1.987	
Cr	0.009	0.008	0.008	0.008	0.008	0.011	0.012	0.009	0.010	
Fe^{2+}	0.565	0.565	0.558	0.566	0.559	0.564	0.566	0.568	0.564	
Fe^{3+}	0	0	0.009	0	0	0	0	0	0	
Mn	0.022	0.022	0.021	0.022	0.021	0.022	0.021	0.020	0.021	
Mg	1.902	1.937	1.943	1.921	1.934	1.939	1.963	1.923	1.924	
Ca	0.463	0.467	0.467	0.467	0.462	0.448	0.451	0.461	0.460	
Mg#	77.1	77.4	77.7	77.2	77.6	77.5	77.6	77.2	77.3	

atmospheric pressure. However, to our knowledge, there is no evidence for widely different effects of these elements on the Fe-C system at pressures of the upper mantle as compared to atmospheric pressure, so that results from atmospheric pressure will be extrapolated here. At atmospheric pressure sulphur lowers the Fe-C eutectic by 25 to 50 °C (Goodrich and Berkley 1986, and references therein), but nickel counterbalances this somewhat by raising temperatures. The overall effect of Ni and S on the position of the eutectic at high pressures is therefore expected to be small.

At pressures within the diamond stability field, cohenite is an incongruently melting intermediate phase in the Fe-C system (Fig. 4). The estimated average bulk composition of the metallic spherules plots at 19 mol% C (4.5 wt%) between the eutectic and peritectic point compositions on the "hypereutectic" side of the phase diagram. For this composition cohenite is the liquidus phase, and is joined by cohenite plus γ-iron at the eutectic. However, unlike in the meteoritic spherules, large cohenite crystals are not observed. A possible reason for the lack of larger cohenite crystals could be that the system cooled rapidly to temperatures below the eutectic where γ-iron and cohenite would crystallize simultaneously or shortly following each other, leading to smaller grain sizes.

The position of the average bulk between peritectic and eutectic is sufficiently close to the peritectic point to suggest that the bulk *spherule* composition is carbon-saturated. Noting that diamond is a major phase, the bulk composition of the system garnet + metallic spherules + diamond would lie between Fe_3C and C, in which case the liquid should remain at the peritectic until all iron crystallizes as Fe_3C. However, if the melt is spatially separated from the excess carbon, as indicated by the occurrence of most spherules as inclusion in the silicate phase, the liquid composition would move further towards the eutectic. The troilite occurring as shells around the metallic spherules exhibits arcuate grain boundaries between metallic core and sulphidic rim, those being more typical for boundaries between two liquids than for those around exsolved sulphide grains. At atmospheric pressure, Fe-S and Fe-C form immiscible liquids in the primary phase field of cohenite at temperatures above the eutectic (Vogel and Ritzau 1931). Goodrich and Berkley (1986) show that for their composition, troilite shells formed from an immiscible Fe-S liquid at temperatures slightly above 1,100 °C. The bulk composition and petrographic similarities between the troilite shells of high-pressure origin in this study and those of low pressure origin of Goodrich and Berkley (1986) strongly suggest a similar process of liquid immiscibility. Small sulphide droplets within the metallic spherules (e.g. Fig. 3b) may have a similar origin (crystallizing as the last phase in interstitial spaces) or, alternatively, represent exsolution features. This, however, remains unresolved, as the sulphides within the spherules are too small to be studied by EPMA.

A lower temperature limit for the formation of the metal-sulphide spherules can be assumed to be around the cohenite liquidus temperature of 1,370 °C at 5.6 GPa (Fig. 4). A maximum upper limit can be derived from the liquidus temperature of anhydrous eclogite which is ca. 1,600 °C at 5 GPa with garnet as the liquidus phase (Yasuda et al. 1994). It will be argued below that crystallization occurred under hydrous conditions so that temperatures closer to 1,370 °C may be more realistic. It appears, therefore, that this polycrystalline diamond aggregate crystallized within the upper range of those typical for diamond formation (950–1,350 °C; Navon, 1999).

Typical morphological features of polycrystalline diamond aggregates (boart) are a high porosity in the form of cavities rimmed by euhedral diamond crystals (e.g. Dobosi and Kurat 2002; Kurat and Dobosi 2000) and small grain size compared to gem-sized stones.

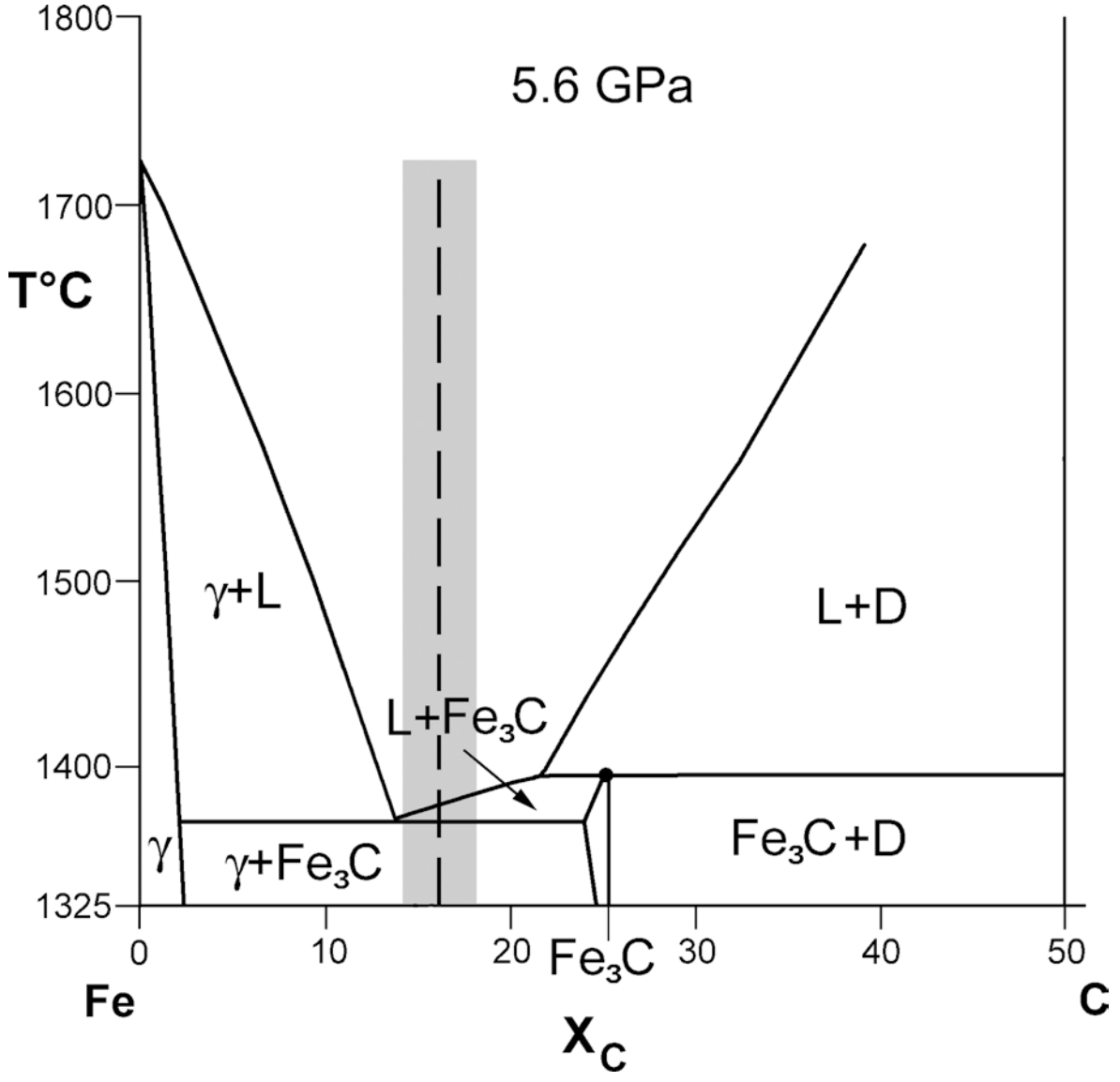

Fig. 4 Phase diagram of the Fe–C system at 5.6 GPa in mol% (modified after Strong and Tuft 1973). The *dashed line* indicates the average bulk composition of the spherules (Table 2) with the *grey box* signifying the 2σ error. The significant differences to the phase diagram at atmospheric pressure are the stabilization of cohenite (Fe_3C), and that the stable native iron modification is γ-iron instead of α-iron at atmospheric pressure. The combined effects of S and Ni are not known at this pressure, but their effects are expected to be roughly counterbalancing as they have opposite effects on the position of the Fe–C eutectic at atmospheric pressure (Goodrich and Berkley 1986)

These features are characteristic for rapid crystallisation from a fluid phase oversaturated in carbon (Gurney and Boyd 1982). Dobosi and Kurat (2002) used trace element compositions of silicate inclusions in framesites to argue for carbonatitic fluids as their source. However, the native iron–carbide–silicate paragenesis in this study requires relatively reducing conditions for crystallization of around the iron-wüstite (IW) oxygen buffer or even well below, whereas carbonatitic fluids or melts are comparatively oxidised (approximately 3–4 orders of magnitudes higher, close to the QFM oxygen buffer; Friel and Ulmer 1974; Green and Falloon 1998; Olafsson and Eggler 1983).

The oxygen fugacities of the majority of inclusions in diamond as well as of mantle rocks from the subcratonic lithosphere range over ca. 6 log units between FMQ and IW (Ballhaus 1993; Navon 1999). However, inclusions in diamond from the Venetia Mine show a distribution of oxygen fugacities that extends to fO_2 of approximately 2 log fO_2 units below IW (Deines et al. 2001), thus, supporting the existence of a low fO_2 environment that manifests itself in these metal-carbide-diamond parageneses.

Formation of cohenite-native iron paragenesis by redox processes

The formation of the unusual carbide–metal–silicate paragenesis reflects local and most likely transient

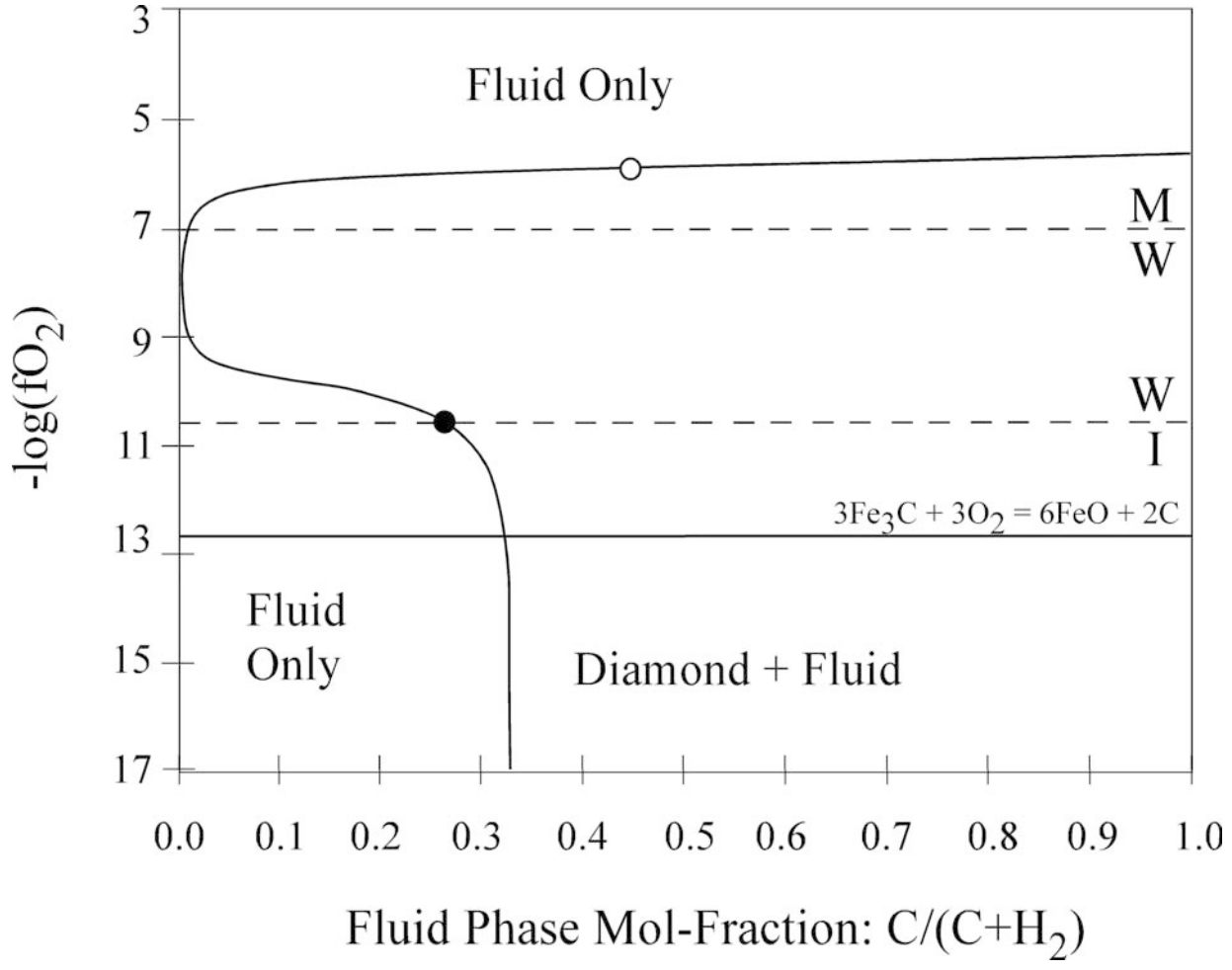

Fig. 5 Log fO_2–X_c diagram for C-O-H fluids in equilibrium with diamond for P = 5.5 GPa, T = 1,400 K (after Taylor 1990). The *heavy curve* delineates the stability field of diamond and coexisting fluid at this P and T. The oxidized fluid-only region lies above, and the reduced fluid-only region to the left of the saturation curve. They are effectively separated by a diamond + fluid field that extends to very water-rich fluid compositions (the "nose" of the diamond saturation curve). Positions of the magnetite-wüstite (*MW*) and the iron-wüstite (*IW*) oxygen buffers (the latter with a *solid circle* at the intersection with the diamond saturation curve as indication for a possible starting composition of the system) are indicated by *dashed lines*. Fluids coexisting with diamond at fO_2 = IW and below consist of mixtures of $CH_4 > H_2O > H_2$ and C_2H_6 progressing to mixtures of $CH_4 > C_2H_6 > H_2$ at fO_2s well below IW. The oxygen fugacity of the principal stability reaction of cohenite, given as $3Fe_3C + 3O_2 = 6FeO + 2C$ is shown for reference. Thermodynamic data taken from Robey and Hemingway (1995). See text for further explanation

conditions within the lithosphere, as polycrystalline diamond aggregates are very rare and the assemblage corresponds to the reducing end of the range of fO_2 found within the Earth's mantle. Trace element zonations in garnets from framesites show that at least some of these rocks must be as young as the kimberlite that transported them (Jacob et al. 2000), implying that the formation of framesites is related to kimberlite ascent.

A plausible scenario for the origin of framesites would be that they form at the ductile to brittle deformation transition zone, at the base of the subcratonic lithosphere, triggered by the opening of cracks related with the upwelling of buoyant material that led to kimberlite magma production. These cracks would serve as pathways for mantle fluids and provide, for a short time, very distinct local conditions, particularly in terms of pressure and oxygen fugacity, in which carbides are able to form. Reduced, CH_4-rich fluids rush into cracks that have transiently markedly lower pressure than their surroundings, but are still within the diamond stability field. This causes immediate oversaturation in diamond, as explained below, and thus drives the reaction $CH_4 + O_2 = C + H_2O$ to the right, resulting in rapid precipitation of diamond as polycrystalline aggregates and redox melting of the silicate components due to rapid H_2O production by the same reaction. Thus, the immediately ensuing precipitation of diamond occurs in a molten environment of short duration, from which the crystallization of garnet, diamond and cohenite occurs as described above (and in Fig. 4).

The composition of C-H-O fluids in equilibrium with carbon at 5.5 GPa and 1,400 K is shown in Fig. 5 (after Taylor 1990). Fluids at low fO_2 (iron-wüstite buffer; IW) are constrained to lie at the position of the solid circle, and are reduced, consisting of 75.6 mol% CH_4, 19.1 mol% H_2O, 2.6 mol% H_2 and 2.7 mol%

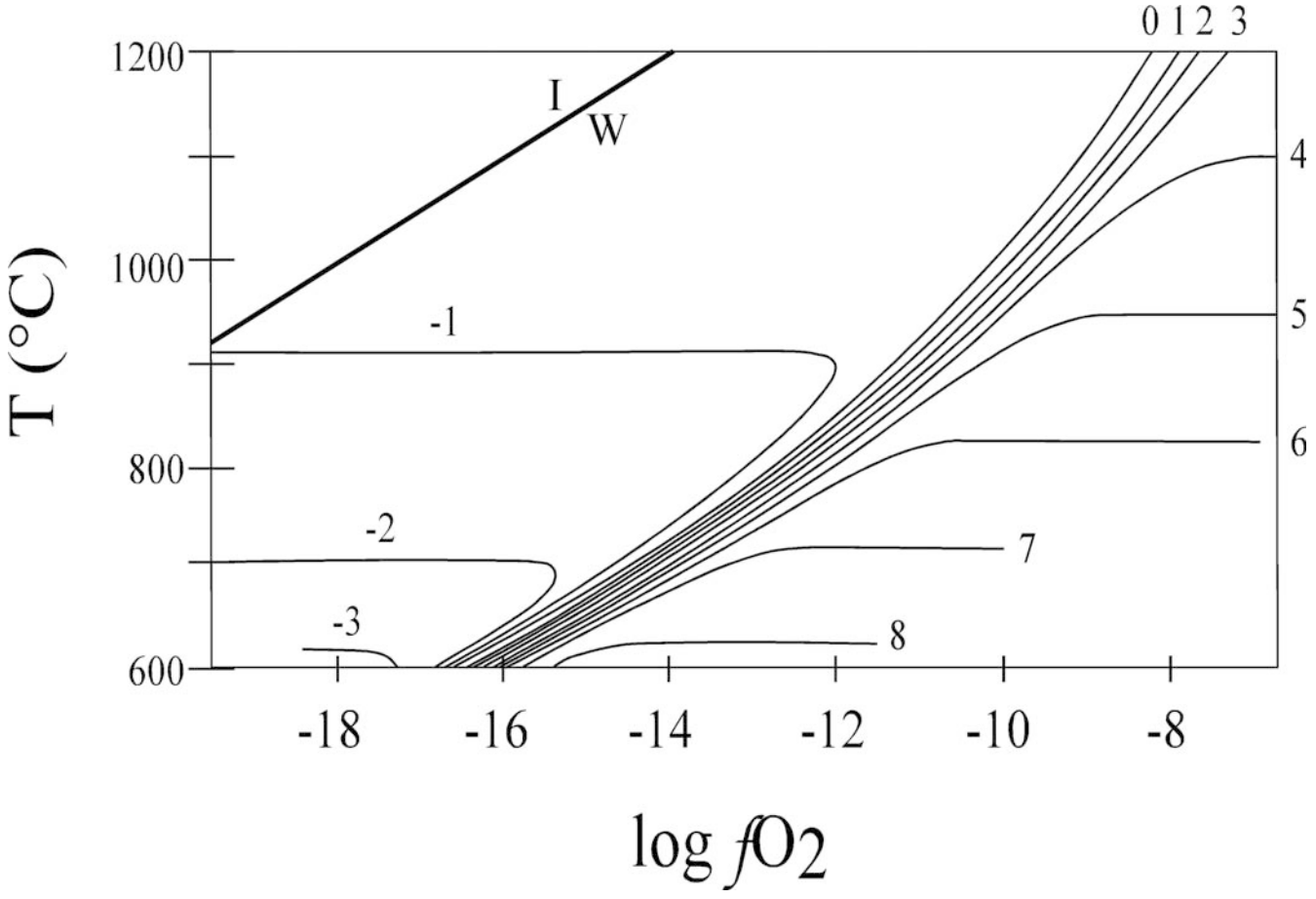

Fig. 6 Carbon isotopic fractionation as a function of temperature and oxygen fugacity at 5 GPa (after Deines 1980). The *curves* represent carbon isotopic fractionation between vapour (CH_4 or CO_2) and diamond with the *numbers* along the curves indicating the numerical values of 1,000 ln $\alpha_{v\text{-}d}$. The iron-wüstite buffer (*IW*, after Schwab and Küstner 1981, with P correction) is plotted for reference. The studied cohenite-native iron-silicate paragenesis plots in the area of minimal fractionation

C_2H_6 (Taylor 1990; Fig. 5). At lower fO_2 than IW fluids become H_2O-poorer and CH_4-richer. In contrast, at high oxygen fugacities, e.g. –log $fO_2 = 5.85$, above the magnetite-wüstite buffer (MW), a fluid in equilibrium with carbon (open circle) is oxidised and consists of approximately equal amounts of H_2O and CO_2. At intermediate fO_2, at the "nose" of the diamond saturation curve in Fig. 5, fluids are very water-rich; at the water maximum, Taylor (1990) gives their composition as 99.6 mol% H_2O with traces of CO_2, CH_4 and H_2. At lower pressures than shown in Fig. 5, the saturation curve moves to lower fO_2 whilst retaining a broadly similar shape, so that the intersection fluid composition indicated by the solid circle in Fig. 5 is moved into the metastable region to the right of the saturation curve and thus suddenly oversaturated in diamond. This forces the production of diamond and water as the fluid composition moves towards the new position of the diamond saturation curve. The H_2O produced causes melting and thus precipitation of diamond, garnet and cohenite from a melt in conditions that were initially subsolidus.

Based on negative $\delta^{13}C$ values an exotic fluid or component of biogenic or crustal origin is often invoked in diamond formation (Deines 2002). Biogenic or crustal material and fluids thereof, however, are rich in nitrogen which is included as diamond grows (Cartigny et al. 1998), whereas the diamonds studied here are nitrogen-free and do not support this hypothesis.

However, during rapid framesite formation the fO_2 may be inhomogeneous on a very local scale, so that a mantle fluid with fO_2 around IW is capable of evolving to lower fO_2 by precipitation of diamond and reaction with surrounding, more oxidised silicate material. As carbon from a fluid in equilibrium with diamond at $fO_2 = IW$ (consisting of $CH_4 > H_2O > H_2$) is consumed by diamond precipitation via the dissociation of methane ($CH_4 = C + 2H_2$), the activity (or the mole fraction) of hydrogen in the remaining fluid increases rapidly, because for each mole of carbon consumed, two moles of H_2 are produced. This progressive change in composition drives the oxygen fugacity of the system to lower values, while water from the fluid induces melting of surrounding silicate material. The hydrogen reduces Ni^{2+}, Co^{2+}, Cu^{2+}, P^{5+} and Fe^{2+} in the silicate melt. Due to the siderophile character of these elements, they partition into a carbon-rich metallic melt and the silicate melt upon solidification crystallizes a garnet depleted in those

elements. It is therefore possible that the system evolved from close to IW to more reducing conditions due to diamond crystallization, probably similar to those given by the stability reaction for cohenite given in Fig. 5.

Deines et al. (2001) took the skewness to lower fO_2 in the range of inclusions in diamond from the Venetia Mine as evidence for a process in which a reduced fluid entered an oxidised environment whose oxidising capacities would slowly be exhausted, which would agree with the scenario developed above.

Unusually reduced environments in the upper mantle can be created locally by mantle processes and an involvement of subducted (biogenic) material is not *a priori* necessary.

Carbon isotopic fractionation between vapour and diamond is very small at $fO_2 = IW$ and below (Fig. 6) and considerable fractionation can only be produced by Rayleigh distillation processes at high vapour/fluid ratios (Cartigny et al. 1998; Deines 1980). The carbon isotopic signature of C-H-O vapour is therefore very likely to be similar to the measured $\delta^{13}C$ value of the diamond of −13.7‰. This value is different from the peak of the carbon isotopic variation found in lherzolitic diamonds, believed to represent mantle carbon (−5‰, e.g. Sobolev et al. 1979; Kirkley et al. 1991), but close to the predicted value for mantle methane of around −15‰ (Kamenskiy et al. 1976) as well as to the measured values for non-biogenic methane from mid-ocean ridges of −15 to −17.6‰ (Welhan and Craig 1983). As opposed to the fluid-derived carbon, the oxygen isotopic signature is introduced by the silicate environment, as this represents a much larger reservoir of oxygen than the fluid. The oxygen isotopic value of 7.2‰ of the garnet supports the view that subducted material is present in the subcratonic lithosphere at Venetia (Aulbach et al. 2002).

Acknowledgments We thank Pierre Cartigny (IPGP Paris) and Nathalie Grassineau (University of London) for providing first class stable isotope analyses. Cyrena Goodrich provided a Disko cohenite standard and gave valuable insights into the metallurgical literature and discussions with Astrid Holzheid and Sharon Webb helped to shape thought regarding oxygen fugacity estimations. Earlier versions of this article profited from informal and formal reviews by Dave Green, Nick Sobolev, Alan Woodland, Ben Harte and Jeff Harris. D.J. gratefully acknowledges financial support from the Deutsche Forschungsgemeinschaft.

References

Allsopp HL, Smith CB, Seggie AG, Skinner EMW, Colgan EA (1995) The emplacement age and geochemical character of the Venetia kimberlite bodies, Limpopo Belt, Northern Transvaal. S Afr J Geol 98(3):239–244

Aulbach S, Stachel T, Viljoen KS, Brey GP, Harris JW (2002) Eclogitic and websteritic diamond sources beneath the Limpopo Belt—is slab-melting the link? Contrib Mineral Petrol 143:56–70

Ballhaus C (1993) Redox states of lithospheric and asthenospheric upper mantle. Contrib Mineral Petrol 114:331–348

Bulanova GP (1995) The formation of diamond. J Geochem Explor 53:1–23

Bulanova GP, Zayakina NV (1990) A graphite-cohenite-iron mineral association in the core of a diamond form the twenty-third Soviet communist party congress pipe. Doklady Akad. Nauk. SSSR, Geoscience section 317:706–709

Cartigny P, Harris JW, Javoy M (1998) Eclogitic diamond formation at Jwaneng: no room for a recycled component. Science 280:1421–1424

Collinson DW (1998) Magnetic properties of polycrystalline diamonds. Earth Planet Sci Lett 161:179–188

Deines P (1980) The carbon isotopic composition of diamonds: relationship to diamond shape, color, occurrence and vapor composition. Geochim Cosmochim Acta 44:943–961

Deines P (2002) The carbon isotope geochemistry of mantle xenoliths. Earth Sci Rev 58:247–278

Deines P, Viljoen F, Harris JW (2001) Implications of the carbon isotope and mineral inclusion record for the formation of diamonds in the mantle underlying a mobile belt: Venetia, South Africa. Geochim Cosmochim Acta 65:813–838

Dobosi G, Kurat G (2002) Trace element abundances in garnets and clinopyroxenes from diamondites—a signature of carbonatitic fluid. Mineral Petrol 76:21–38

Eggler DH (1983) Upper mantle oxidation state: evidence from olivine-orthopyroxene-ilmenite assemblages. Geophys Res Lett 10:365–368

Friel JJ, Ulmer GC (1974) Oxygen fugacity geothermometry of the oka carbonatite. Am Mineral 59:314–318

Goodrich CA, Berkley JL (1986) Primary magmatic carbon in ureilites; evidence from cohenite-bearing metallic spherules. Geochim Cosmochim Acta 50(5):681–691

Goodrich CA, Bird JM (1985) Formation of iron-carbon alloys in basaltic magma at Uivfaq, Disko Island; the role of carbon in mafic magmas. J Geol 93(4):475–492

Green D, Falloon T (1998) Pyrolite: a Ringwood concept and its current expression. In: Jackson I (ed) The Earth's mantle. Cambridge University Press, New York, pp 311–378

Gurney JJ, Boyd FR (1982) Mineral intergrowths with polycrystalline diamonds from the Orapa Mine, Botswana. Carnegie Inst Year Book, pp 267–273

Haggerty SE, Tompkins LA (1986) Redox state of the Earth's upper mantle form kimberlitic ilmenites. Nature 303:295–300

Henke BL, Lee P, Tanaka TJ, Shimabukuro RL, Fujikaawa BK (1982) Low-energy x-ray interaction coefficients: photoabsorption, scattering, and reflection. At Data Nucl Data Tables 27:1–144

Irmer W (1920) Der Basalt des Bühls bei Kassel und seine Einschlüsse von Magnetit, Magnetkies und gediegen Eisen. Abhdl Senckenb Naturf Ges 137:91–108

Jacob DE, Foley SF (1999) Evidence for Archean ocean crust with low high field strength element signature from diamondiferous eclogite xenoliths. Lithos 48:317–336

Jacob DE, Schmickler B, Schulze DJ (2003) Trace element geochemistry of coesite-bearing eclogites from the Roberts Victor kimberlite, Kaapvaal craton. Lithos (in press)

Jacob DE, Viljoen KS, Grassineau N, Jagoutz E (2000) Remobilization in the cratonic lithosphere recorded in polycrystalline diamond. Science 289:1182–1185

Kamenskiy IL, Lobkov VA, Prasolov EM, Beskrovny NS, Kudryavtseva EI, Anufriev GS, Pavlov VB (1976) The components of the upper mantle of the Earth in gases of Kamchatka (according to He, Ne, Ar and C isotopy). Geochem Int 13:35–48

Kirkley MB, Gurney JJ, Otter ML, Hill SJ, Daniels LR (1991) The application of C isotope measurements to the identification of the sources of C in diamonds: a review. Appl Geochem 6:477–494

Kirkley MB, Gurney JJ, Rickard RS (1995) Jwaneng Framesites: Carbon isotopes and intergrowth compositions. In: Meyer HOA, Leonardos OH (eds) Diamonds: characterization, genesis and exploration, Vol. 2. CPRM Spec Publ 1/95, pp 127–135

Kurat G, Dobosi G (2000) Garnet and diopside-bearing diamondites (framesites). Mineral Petrol 69:143–160

Leung IS, Guo W, Friedman I, Gleason J (1990) Natural occurrence of silicon carbide in diamondiferous kimberlite from Fuxian. Nature 346:352–354

Lovering JF (1964) Electron microprobe analysis of terrestrial and meteoritic cohenite. Geochim Cosmochim Acta 28(11):1745–1755

Mathez EA, Fogel RA, Hutcheon ID, Marshintsev VK (1995) Carbon isotopic composition and origin of SiC from kimberlites of Yakutia. Geochim Cosmochim Acta 59:781–791

Mattey D, Macpherson C (1993) High-precision oxygen isotope microanalysis of ferromagnesian minerals by laser-fluorination. Chem Geol 105:305–318

McCandless TE, Kirkley MB, Robinson DN, Gurney JJ, Griffin WL, Cousens DR, Boyd FR (1989) Some initial observations on polycrystalline diamonds mainly from Orapa: Abstract. Ext. Abstr. 28th Int Geological Congress, pp 47–51

Moore RO, Gurney JJ (1986) Mineral inclusions in diamond from the Monastry kimberlite, South Africa. In: Ross J, Jaques AL, Ferguson J, Green DH, O'Reilly SY, Danchin RV, Janse AJA (eds) Kimberlites and related rocks, Vol. 14. Geol Soc Austr Spec Publ, pp 1029–1041

Navon O (1999) Diamond formation in the Earth's mantle. In: Gurney J, Gurney JL, Pascoe MD, Richardson SH (eds) Proc 7th Int Kimberlite Conf, Vol 2, pp 584–604

Newbury DE, Myklebust RL (1995) NIST Micro MC: a user's guide to the NIST Microanalysis Monte Carlo electron trajectory simulation program. Microbeam Anal 4:165–175

Nisbet EG, Mattey DP, Lowry D (1994) Can diamonds be dead bacteria? Nature 367, p 694

O'Neill HSC, Wall VJ (1987) The olivine-orthopyroxene-spinel oxygen geobarometer, the nickel precipitation curve, and the oxygen fugacity of the Earth's upper mantle. J Petrol 28:1169–1191

Olafsson M, Eggler D (1983) Phase relations of amphibole, amphibole-carbonate, and phlogopite-carbonate peridotite: petrologic constraints on the asthenosphere. Earth Planet Sci Lett 64:305–315

Orlov JL (1977) The mineralogy of diamond. Wiley, New York, 235 pp

Petch NJ (1944) The interpretation of the crystal structure of cementite. J Iron Steel Indust 149:143–150

Robey RA, Hemingway BS (1995) Thermodynamic properties of minerals and related substances at 298.15 K and 1 bar (10^5 Pascals) pressure and at higher temperatures. US Geol Surv Bull 2131. US Department of the Interior, Washington, DC, 461 pp

Schwab RG, Küstner D (1981) The equilibrium fugacities of important oxygen buffers in technology and petrology. Neues Jahrb Mineral Abh 140:111–142

Sharp WE (1966) Pyrrhotite: a common inclusion in South African diamonds. Nature 211:402–403

Sobolev NV, Pokhilenko NP, Lavrent'ev YG, Usova LV (1975) Distinctive features on the composition of chrome spinels in the diamonds and kimberlites of Yakutia. Soviet Geol Geophys 16(11):7–24

Sobolev NV, Galimov EM, Ivanovskaya I, Yefimova ES (1979) The carbon isotope compositions of diamonds containing crystalline inclusions (in Russian). Dokl Akad Nauk SSSR 249:1217–1220

Sobolev NV, Yefimova ES, Pospelova LN (1989) Native iron in Yakutian diamonds and its paragenesis. Soviet Geol Geophys 22:18–21

Stachel T, Harris JW, Brey GP (1998) Rare and unusual mineral inclusions in diamonds from Mwadui, Tanzania. Contrib Mineral Petrol 132:34–47

Strong HM, Tuft RE (1973) The Fe-C system at ~56 kb. General Electric. Technical Information Series, Report no 73CRD244:1–3

Taylor WR (1990) A reappraisal of the nature of fluids included by diamond—a window to deep-seated mantle fluids and redox conditions. In: Herbert HK, Ho SE (eds) Stable isotopes and fluid processes in mineralization. University of Western Australia, pp 333–349

Ulff-Møller F (1985) Solidification history of the Kitdilt Lens; immiscible metal and sulphide liquids from a basaltic dyke on Disko, central West Greenland. J Petrol 26(1):64–91

Vogel R, Ritzau G (1931) Über das ternäre System Eisen-Schwefel-Kohlenstoff. Archiv für das Eisenhüttenwesen 4:549–556

Welhan JA, Craig H (1983) Methane, hydrogen and helium in hydrothermal fluids at 21°N on the East Pacific Rise. In: Rona PA, Bostrom K, Laubier L (eds) Hydrothermal processes at seafloor spreading centers 12. Plenum Press, New York, pp 391–410

Wood BJ (1993) Carbon in the core. Earth Planet Sci Lett 117:593–607

Yasuda A, Fujii T, Kurita K (1994) Melting phase-relations of an anhydrous midocean ridge basalt from 3 to 20 GPa—Implications for the behavior of subducted oceanic crust in the mantle. J Geophys Res 99(B5):9401–9414